

# Cosmogenic and nucleogenic $^3\text{He}$ in apatite, titanite, and zircon

K.A. Farley <sup>a,\*</sup>, J. Libarkin <sup>b</sup>, S. Mukhopadhyay <sup>c</sup>, W. Amidon <sup>a</sup>

<sup>a</sup> Division of Geological and Planetary Sciences, California Institute of Technology, MS 170-25, Caltech, Pasadena, CA 91125, USA

<sup>b</sup> Department of Geological Sciences, Ohio University, Athens, OH 45701, USA

<sup>c</sup> Department of Earth and Planetary Sciences, Harvard University, Cambridge, MA 02138, USA

Received 7 April 2006; received in revised form 6 June 2006; accepted 6 June 2006

Available online 17 July 2006

Editor: R.W. Carlson

## Abstract

Cosmogenic  $^3\text{He}$  was measured in apatite, titanite, and zircon and cosmogenic  $^{21}\text{Ne}$  in quartz at 13 depth intervals in a 2.7-m long drill core in a Miocene ignimbrite from the Altiplano of Bolivia. All three  $^3\text{He}$  depth profiles as well as the  $^{21}\text{Ne}$  profile attenuate exponentially with depth, indicating that both of these isotopes are cosmogenic in origin with no significant contribution from other sources. The attenuation lengthscale for  $^3\text{He}$  production of  $A = 180 \pm 11 \text{ g/cm}^2$  is consistent with expectations for neutron spallation, and is identical to that found for the cosmogenic  $^{21}\text{Ne}$  in quartz. By normalizing the measured  $^3\text{He}$  concentrations to  $^{21}\text{Ne}$  and using the independently known cosmogenic  $^{21}\text{Ne}$  production rate, the apparent cosmogenic  $^3\text{He}$  production rates in apatite, titanite, and zircon were respectively found to be 112, 97, and 87 atoms/g/yr at sea-level and high latitude. The formal uncertainty on these estimates is  $\sim 20\%$  ( $2\sigma$ ), and arises in equal parts from uncertainties in the measured  $^3\text{He}/^{21}\text{Ne}$  ratios and the uncertainty in the  $^{21}\text{Ne}$  production rate. However an additional factor affecting the apparent  $^3\text{He}$  production rate in these phases arises from the long stopping range of spalled  $^3\text{He}$  and tritium (which decays to  $^3\text{He}$ ). Because all three accessory phases have higher mean atomic number than major rock-forming minerals, they will have lower  $^3\text{He}$  production rates than their surroundings. As a consequence the long stopping ranges will cause a net implantation of  $^3\text{He}$  and therefore higher apparent production rates than would apply for purely in-situ production. Thus these apparent production rates apply only to the specific grain sizes analyzed. Analysis of sieved zircon aliquots suggests that a factor of 2 increase in grain size (from  $\sim 50$  to  $\sim 100 \mu\text{m}$  cross-section) yields a 10% decrease in apparent production rate. While this effect warrants further study, the grain sizes analyzed here are typical of the accessory phases commonly encountered, so the apparent rates provide an appropriate starting place for surface exposure dating using  $^3\text{He}$  in these minerals.

© 2006 Elsevier B.V. All rights reserved.

**Keywords:** cosmogenic helium; apatite; zircon; titanite; production rate; Altiplano

## 1. Introduction

The last few years have seen rapid development of surface exposure dating using the cosmogenic radionuclides  $^{10}\text{Be}$ ,  $^{26}\text{Al}$ , and  $^{36}\text{Cl}$  [1–3]. Less work has been done with stable cosmogenic isotopes such as  $^3\text{He}$  and

$^{21}\text{Ne}$  despite the comparatively good detection limits and the ease with which noble gases can be measured. In the case of  $^{21}\text{Ne}$ , the major limitation is nucleogenic neon from U and Th decay [4]. For  $^3\text{He}$ , there are two recognized limitations. Non-cosmogenic helium is commonly found in minerals either from the reaction  $^6\text{Li}(n,\alpha)^3\text{H} \rightarrow ^3\text{He}$  or from the presence of mantle helium in fluid inclusions [4]. More importantly, many rock-forming minerals do not retain helium against diffusion at earth surface temperatures. For

\* Corresponding author.

E-mail address: [farley@gps.caltech.edu](mailto:farley@gps.caltech.edu) (K.A. Farley).

example, quartz [5] and feldspar [6] leak helium at 20 °C, while biotite and hornblende commonly have 10s of ppm of Li [7], which can yield substantial nucleogenic  $^3\text{He}$  over time. These factors have restricted surface exposure dating using  $^3\text{He}$  almost exclusively to young basalts bearing olivine or pyroxene phenocrysts (e.g., [4,8]).

More recently other mineral phases have come under investigation for  $^3\text{He}$ -based exposure dating, including garnet [9] and magnetite [6]. Here we expand on this work by establishing a framework for surface exposure dating using cosmogenic  $^3\text{He}$  in three accessory phases: apatite ( $\text{Ca}_5(\text{PO}_4)_3\text{F}$ ), titanite (“sphene”,  $\text{CaTiSiO}_5$ ) and zircon ( $\text{ZrSiO}_4$ ). These minerals are ubiquitous and retain He under earth surface conditions [10]. Cosmogenic  $^3\text{He}$  has been detected in igneous apatites from the Dry Valleys of Antarctica, and in fossil tooth enamel apatite [11], but there appear to be no reports of cosmogenic helium in titanite or zircon. Here we describe results from a 2.7-m long depth profile of  $^3\text{He}$  measurements in these three phases. Our goal is to establish that cosmogenic  $^3\text{He}$  is present in these minerals, to assess the mechanism by which it is produced, and to obtain an estimate of the  $^3\text{He}$  production rates. We then consider several factors which may complicate cosmogenic dating of these phases.

## 2. Samples and methods

We analyzed samples from a core drilled into a thick ignimbrite on the Bolivian Altiplano. The ignimbrite was selected for its high abundance of apatite, titanite, and zircon, plus quartz for  $^{21}\text{Ne}$  measurement. The ignimbrite was sampled at 18° 15.694' S, 68° 14.702' W, elevation 3843 m. It likely corresponds to sample 90BR037 reported by du Bray et al. [12], who provide major element data for this ignimbrite. As discussed below, it is Miocene in age and has an apparent exposure age based on  $^{21}\text{Ne}$  in quartz of ~ 100 kyr, indicating significant erosion. The ignimbrite is a moderately welded rhyolite ash-flow forming a laterally extensive, flat, continuously exposed surface. A total of 2.7 m of core was drilled in sections ranging in length from 2 to 40 cm, with drilling-related loss of approximately 40 cm from the lower two-thirds of the core. Depths above 150 cm are exact to  $\pm 5$  cm, and depths below are exact to  $\pm 10$  cm. Core sections were cut into 2–4 cm pieces, from which 13 samples were processed for heavy minerals.

Segments of core totaling 2 to 10 cm in length were crushed to pea-gravel size, and apatite, titanite and zircon were purified using standard heavy liquid and magnetic techniques. The resulting apatite separate was visually pure and aliquots were analyzed without further prepara-

tion. The analyzed grains were generally small (~ 50  $\mu\text{m}$  in cross-section) and were a mixture of euhedral crystals and fragments. The titanite separate was sieved at 150  $\mu\text{m}$ , and the coarse fraction was handpicked to exclude contaminants. The average cross-section of the analyzed grains was 250  $\mu\text{m}$ ; most were fragments of originally larger grains. The zircon separate was heavily contaminated with titanite, so it was placed in a mixture of 2:1 concentrated HF/HNO<sub>3</sub> and heated to boiling in an open beaker for 1 h. The acid was replaced with concentrated HCl and heated for an additional hour. This heating will not release He from zircon [13]. The resulting separate was found to be pure zircon. Individual euhedral grains averaging ~ 110  $\mu\text{m}$  in cross-section were handpicked and analyzed. After these samples were analyzed we recognized a possible role of grain size on the cosmogenic  $^3\text{He}$  production rate, so for one sample (D1\_D2) we obtained a second zircon sample and sieved it into two size fractions. Based on measurements of at least 100 grains the mass-weighted mean grain cross section of the coarse fraction was 91  $\mu\text{m}$ , and for the fine fraction, 53  $\mu\text{m}$ . Most but not all grains were euhedral prisms rather than fragments.

Helium was extracted by laser heating of 2 to 10 mg of separate contained in 6-mm lengths of 3-mm OD Pt–10%Ir tubing (Johnson Matthey Medical P/N 10170). Prior to use the tubing was annealed and degassed by in-vacuum laser heating to incandescence. Each length of tubing can hold about 2 mg of separate, so larger aliquots were divided among multiple tubes. After loading, the tube ends were crimped and the aliquots were placed into a vacuum chamber below a sapphire viewport. Following 12 h of evacuation each aliquot was heated with a Nd-YAG laser to ~ 1300 °C for 15 min. During this period the laser power was controlled by monitoring the brightness of the packet to maintain the desired temperature, and the beam was rastered across the tubes to ensure uniform degassing. All helium is extracted from these minerals at this temperature [10] as confirmed by a second heating and analysis of several samples. The evolved helium was purified, cryofocussed, and separated from Ne using standard procedures at Caltech [14]. The helium was admitted into a MAP 215-50 mass spectrometer and the two isotopes analyzed by peak-jumping.  $^3\text{He}$  was detected on a pulse-counting electron multiplier.

Laser extraction blanks were close to the detection limit for  $^3\text{He}$  (~ 3000 atoms) and were  $< 2 \times 10^9$  atoms for  $^4\text{He}$ . In all cases the  $^4\text{He}$  blanks were negligible (<1%). The  $^3\text{He}$  blank was  $\ll 1\%$  for most samples, reaching a maximum of 5% on the samples from deepest in the core. The  $^3\text{He}$  abundance was determined by peak

height comparison with gas standards. Linearity of  $^3\text{He}$  peak heights was established by analyzing standards of known size; these standards encompassed the amount of  $^4\text{He}$  present in the mass spectrometer during sample analyses. Analytical uncertainties for  $^3\text{He}$  concentration were computed from the observed reproducibility of standards of comparable beam size, added in quadrature to the uncertainty in the blank correction (assumed to be 100%).

Quartz samples for neon analysis were crushed to 0.4–1 mm cross-section and leached in dilute HCl to eliminate feldspars. The leached material was inspected with a binocular microscope at Harvard and grains with obvious inclusions were rejected. Aliquots of between 130 and 214 mg of quartz were wrapped in tantalum foil and loaded in a vacuum furnace in the noble gas laboratory at Harvard. The furnace was pumped and baked for 36 h at 120 °C, except for the sample arms, which were kept at  $\sim 45$  °C for 12 h. After completion of the bakeout the furnace was pumped until the neon blanks stabilized (usually within 2–4 days). After heating for 15 min, evolved gases were purified by sequential exposure to SAES getters at 450 °C and room temperature. Neon was adsorbed on a cryogenic cold finger at 33 K, released at 74 K, and inlet to the mass spectrometer. Neon isotopes were measured with the Nu Noblesse mass spectrometer at Harvard (Mukhopadhyay, in preparation). All three neon isotopes were measured on electron multipliers operating in pulse-counting mode. The  $\text{Ar}^{++}/\text{Ar}^+$  ratio was  $0.088 \pm 0.001$  and was independent of Ar,  $\text{CO}_2$ , and  $\text{H}_2$  partial pressures. The  $\text{CO}_2^{++}/\text{CO}_2^+$  ratio was found to be dependent on both  $\text{CO}_2$  partial pressure and the  $\text{H}_2$  partial pressure. As a result  $\text{H}_2$  was monitored during each analysis. For typical operating conditions  $\text{CO}_2^{++}/\text{CO}_2^+$  was  $\sim 0.007$ . Neon abundance and isotopic ratios were determined by comparison to air neon. The  $1\sigma$  variation of standards the same size as the samples was 0.3% for  $^{20}\text{Ne}$ , 0.4% for  $^{21}\text{Ne}/^{20}\text{Ne}$  ratios, and 0.2% for  $^{22}\text{Ne}/^{20}\text{Ne}$  ratios. Typical furnace blanks for  $^{20}\text{Ne}$  were  $\sim 4.5 \times 10^7$  atoms at 1500 °C and  $1.4 \times 10^7$  atoms at 600 °C. Because we used tantalum foil to wrap the samples, neither the foil wrapper nor the sample melted. As a result, blank values remained low and fairly constant over the course of the run. Typically, each 1500 °C temperature step for a sample was followed by two blanks at 1500 °C. Uncertainties for blank corrections were computed from the reproducibility of the blanks bracketing the sample. Reported uncertainties reflect both the reproducibility of the standards and the uncertainties in the blank correction. The uncertainties in the measured values are dominated by uncertainties in the blank

correction. Cosmogenic  $^{21}\text{Ne}$  concentrations were calculated assuming a two-component mixture of cosmogenic and air neon.

A single 5 grain aliquot of apatite from segment C3\_C4 of the core was analyzed for U and Th using procedures developed for (U–Th)/He dating [10]. By combination with the measured  $^4\text{He}$  in the apatites, these concentrations provide a (U–Th)/He (eruption) age for the ignimbrite.

Ignimbrite density was estimated through standard liquid paraffin techniques wherein samples are weighed, coated with liquid paraffin, reweighed and then immersed in water for volume determination [15]. Ten samples distributed along the length of the core were analyzed, with a resulting density and standard deviation of  $1.68 \pm 0.12$  g/cm<sup>3</sup>.

### 3. Results

$^3\text{He}$  and  $^{21}\text{Ne}$  results are presented in Table 1 and Fig. 1. Full isotopic data are included in the supplementary material. In all three accessory phases the  $^3\text{He}$  concentrations decrease systematically down-core, with surface concentrations of about 75–110 Matoms/g decreasing to 7–10 Matoms/g at 250 cm depth. In contrast to  $^3\text{He}$ , the  $^4\text{He}$  concentrations are essentially uniform with depth. Mean  $^4\text{He}$  concentrations averaged across all core segments are 0.48 nmol/g in apatite, 2.7 nmol/g in titanite, and 11 nmol/g in zircon. Coupled with the apatite U and Th concentrations of 7 and 41 ppm respectively, the He concentration implies an  $\alpha$ -ejection corrected (U–Th)/He age for the ignimbrite of about 7.5 Ma.  $^3\text{He}/^4\text{He}$  ratios correlate with depth and mineral phase, and range from a maximum of  $\sim 3 \times 10^{-7}$  in the shallowest apatite sample to a minimum of  $\sim 1 \times 10^{-9}$  in the deepest zircon sample.

If the  $^3\text{He}$  in these samples is cosmogenic and is predominantly produced by a single mechanism (e.g., neutron spallation), then the depth profiles will obey the relationship  $C = C_0 e^{-\rho Z/\Lambda}$  where  $\Lambda$  is the attenuation lengthscale of cosmogenic production,  $C_0$  is the surface concentration,  $Z$  is sample depth and  $\rho$  is rock density. Fig. 2 shows that when  $\ln C$  is plotted against  $\rho Z$ , all three phases display highly linear relationships consistent with this equation. Table 2 shows the results of an error-weighted least squares fit to each of these arrays. The resulting best fit  $\Lambda$  values are the same within error for apatite, titanite, and zircon. Taken together the three phases define an error-weighted mean  $\Lambda$  for  $^3\text{He}$  production at this site of  $180 \pm 11$  g/cm<sup>2</sup> (all errors presented here are  $2\sigma$ ).

These fits also allow estimation of  $C_0$ , the concentration of  $^3\text{He}$  expected in each phase at the top of the core (Table 2). From these estimates the relative

Table 1  
 $^3\text{He}$  concentration data

Sample	Depth (cm)	Apatite $^3\text{He}$		Titanite $^3\text{He}$		Zircon $^3\text{He}$		Quartz $^{21}\text{Ne}$	
		Matom/g	$\pm\sigma$	Matom/g	$\pm\sigma$	Matom/g	$\pm\sigma$	Matom/g	$\pm\sigma$
A	1	110.7	4.6			78.7	8.0		
C3_C4	14	84.3	2.7	73.6	2.7	66.5	3.2	17.0	0.5
C7_C8	22	81.3	3.0	71.3	2.7	60.0	2.7		
D1_D2 c	35	73.7	3.3	64.8	2.5	55.7	2.7	13.7	0.1
D1_D2 m	35					63.7	3.1		
D1_D2 f	35					64.4	2.6		
E5_E7	50	60.8	2.4	54.3	2.4	49.5	2.7	10.3	0.1
H1_H2	74	48.9	1.8			34.0	2.4		
H9_H10	98	40.3	1.8	33.4	2.5	31.3	2.6	6.9	0.1
K1_K2	132	28.1	1.7			20.0	2.4		
M	148	28.8	1.9	21.8	2.7	19.9	2.5	4.4	0.1
P1_P2	164	16.0	1.6	18.7	3.2	15.7	3.6		
Q3_Q4	177	17.1	1.5	18.0	3.4	15.4	2.7	3.4	0.2
R1_R2	244	11.0	1.3	10.4	3.4	8.9	3.6		
T	250	9.7	1.1	9.9	3.6	7.3	3.2	1.8	0.2

c=coarse (111  $\mu\text{m}$  mean grain cross-section); m=medium (91  $\mu\text{m}$ ); f=fine (53  $\mu\text{m}$ ).

concentration of  $^3\text{He}$  in each phase can be deduced. As shown in Table 2, relative to an apatite  $^3\text{He}$  concentration of 1, the concentration in titanite is  $0.86\pm 0.08$  and in zircon is  $0.76\pm 0.08$ .

Fig. 3 shows that the Ne isotopic compositions of the quartz samples plot on a linear array bounded by atmospheric Ne and the previously proposed cosmogenic Ne composition in quartz [16]. Based on this relationship we deconvolved the  $^{21}\text{Ne}$  into atmospheric and cosmogenic components. In the several samples that were step-heated, all steps contained cosmogenic  $^{21}\text{Ne}$ , so we consider only the total for these samples. Cosmogenic Ne accounted for between 13% and 90% of the  $^{21}\text{Ne}$  in the samples. Cosmogenic  $^{21}\text{Ne}$  ( $^{21}\text{Ne}_c$ ) concentrations range from about 2 to 17 Matoms/g, decreasing with depth just like the  $^3\text{He}$  (Fig. 1). This similarity is further reinforced in Fig. 2, where  $\ln ^{21}\text{Ne}_c$  is highly linear with

depth and yields a very similar attenuation length scale to that observed for  $^3\text{He}$  (Table 2).

#### 4. Discussion

He and Ne isotopic data from this core have a number of implications for cosmic ray exposure dating using  $^3\text{He}$  in apatite, titanite, and zircon. Here we establish the probable sources of  $^3\text{He}$  and indirectly calculate the cosmogenic  $^3\text{He}$  production rate by reference to the known production rate of  $^{21}\text{Ne}$  in quartz.

The  $^{21}\text{Ne}$  concentrations in the core behave as expected for cosmogenic Ne (Fig. 2). Based on the  $^{21}\text{Ne}_c$  value extrapolated to the top of the core, a production rate at sea level and high latitude (SLHL) of  $20.3\pm 3.7$  atoms/g/yr [17], and the scaling model of Lal [2], the apparent age of the sampled surface assuming no erosion or cover is  $104\pm$

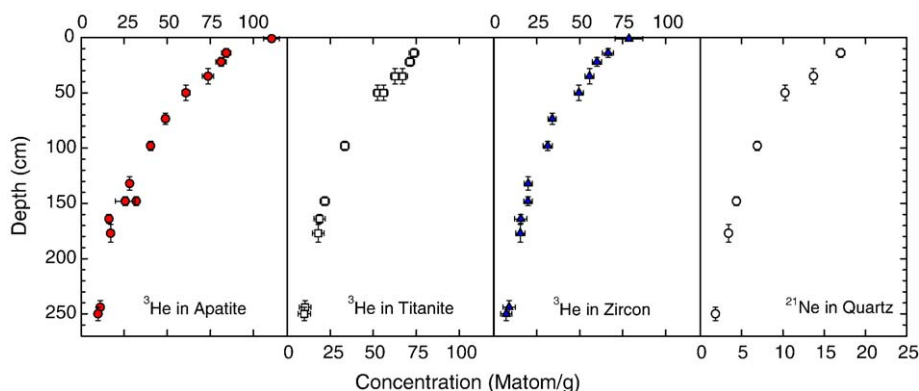


Fig. 1. Total  $^3\text{He}$  in apatite, titanite and zircon and cosmogenic  $^{21}\text{Ne}_c$  in quartz as a function of depth in the ignimbrite drill core. Plotted uncertainties are  $2\sigma$ .

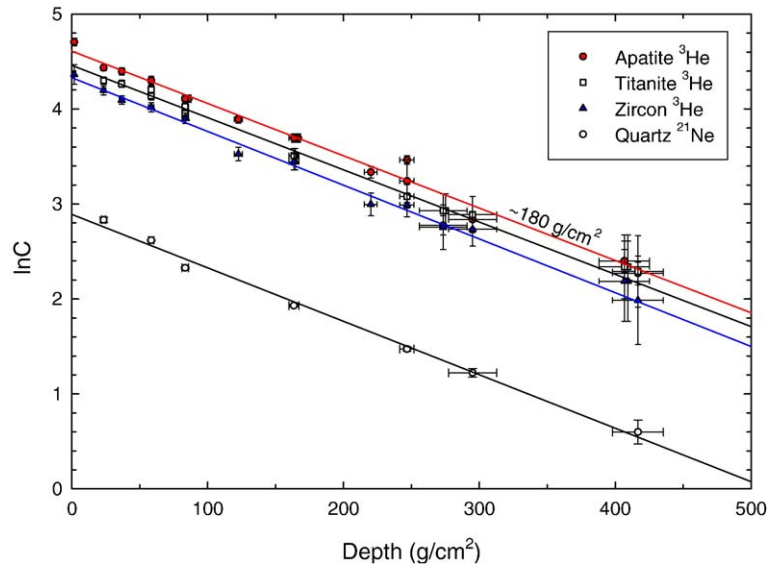


Fig. 2. Natural logarithm of total  $^3\text{He}$  in apatite, titanite and zircon and cosmogenic  $^{21}\text{Ne}_c$  in quartz plotted as a function of the product of density and depth. Regression lines through results for each mineral phase are plotted. All four arrays are highly linear and consistent with an attenuation lengthscale of  $180 \text{ g/cm}^2$ .

22 kyr. The best fit attenuation length scale of  $A=178 \pm 16 \text{ g/cm}^2$  is slightly higher than previous work on other cosmogenic isotope systems, which indicate an attenuation length-scale of cosmic ray neutron reactions of  $150$  to  $170 \text{ g/cm}^2$  [4,18–21]. Our slightly higher value is consistent with the harder cosmic ray energy spectrum expected at the higher elevation and lower latitude of the Bolivia site compared to the reference values. There is no evidence of a significant contribution of cosmogenic components with longer attenuation lengths (e.g., from muons), nor of any non-cosmogenic component other than atmospheric neon.

The data presented in Figs. 1 and 2 provide strong evidence that the  $^3\text{He}$  measured in the accessory phases is also exclusively produced by cosmic ray interactions. Most notable is the strong linearity of the  $^3\text{He}$  profiles in

Fig. 2, and their similarity in attenuation length both to each other and to the unambiguously cosmogenic  $^{21}\text{Ne}_c$ . The absence of systematic residuals to the fits in Fig. 2 suggest that non-cosmogenic He, e.g., in fluid inclusions or from neutron reactions on  $^6\text{Li}$ , are negligible. Therefore we believe that all  $^3\text{He}$  in these samples is in fact cosmogenic, and given the attenuation lengthscale, is overwhelmingly the product of neutron spallation.

Based on the  $C_0$  values for  $^{21}\text{Ne}_c$  in quartz and  $^3\text{He}$  in the three accessory phases, we can estimate the cosmogenic  $^3\text{He}/^{21}\text{Ne}_c$  production ratio for this locality: 4.3, 4.8, and 5.5 for zircon, sphene, and apatite respectively (Table 2). Again taking Niedermann's [17] value for the  $^{21}\text{Ne}_c$  production rate in quartz, we infer apparent SLHL production rates of  $^3\text{He}$  of 87, 97, and 112 atoms/g/yr in zircon, titanite and apatite, respectively. The  $2\sigma$

Table 2  
Summary data

Mineral	Surface concentration		Attenuation lengthscale				P $^3\text{He}$	
	Mat/g	$\pm 2\sigma$	$\text{g/cm}^2$	$\pm 2\sigma$	$^3\text{He}/^{21}\text{Ne}$	$\pm 2\sigma$	Mat/g/ySLHL	$\pm 2\sigma$
$^3\text{He}$								
Apatite	100.5	7.7	181.5	19.7	5.5	0.4	112	24
Titanite	86.5	4.6	181.8	21.1	4.8	0.2	97	19
Zircon	75.9	4.8	176.7	19.6	4.3	0.4	87	18
$^{21}\text{Ne}$								
Quartz	18.0	2.0	177.6	15.9				

Surface concentrations were obtained by extrapolation of depth profile, Fig. 2.

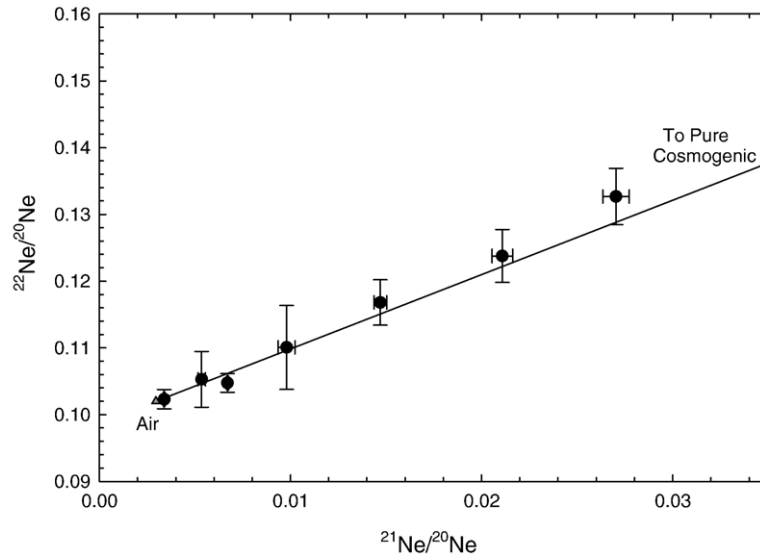


Fig. 3. Neon isotopic data for quartz. All samples plot on the line connecting the air composition with that of pure cosmogenic neon in quartz. This relationship validates a two-component deconvolution for the calculation of cosmogenic  $^{21}\text{Ne}_c$  in these samples.

uncertainty on the apparent production rates is about 20%, arising in equal proportions from the uncertainty in the  $^{21}\text{Ne}_c$  production rate and from the  $^3\text{He}/^{21}\text{Ne}_c$  ratios inferred from the core. We refer to these as apparent production rates because they may not reflect true in-situ production rates for reasons discussed below.

For comparison Table 3 presents predicted  $^3\text{He}$  production rates in common minerals and a rock of granitic composition. These production rates are based on published element-specific rates [20,22]. For elements not compiled in [20,22], we estimated elemental production rates via an empirical linear correlation between the tabulated production rates and the log of the atomic number (obtained values: 136, 118, 92, 71, 59, 8 atoms  $^3\text{He}/\text{g}/\text{yr}$  for F, Na, P, K, Ti and Zr, respectively). For elements other than Zr we would obtain almost the same value by using the production rate linearly interpolated

Table 3  
Predicted production rates

Material	Predicted SLHL prod rate (atoms/g/yr)
Apatite	98
Titanite	98
Zircon	68
Alkali Feldspar	123
Plagioclase	116
Hornblende	119
Biotite	120
Quartz	124
“Granite”	120

Note: predicted production rates are based on element specific production [22] as described in the text.

between neighboring elements. There is greater uncertainty for Zr because it has a much higher atomic number than the elements tabulated [22], so the predicted rate for zircon should be interpreted cautiously. The purpose of this tabulation is not to argue for any specific production rate, but to illustrate some of the issues raised by our data.

The apparent production rates measured in the Bolivian core are in reasonable agreement with these predictions. However, one important factor that must be considered is that the production rates in these phases are all significantly lower than in common rock-forming minerals (Table 3). This occurs because the accessory phases have higher concentrations of high Z elements (Ca, Ti, Zr) that produce smaller amounts of cosmogenic  $^3\text{He}$  than low Z elements. After the analyses plotted in Figs. 1 and 2 were performed we realized that the distinction in production rate between the analyzed minerals and their host rock could have important consequences that cause the apparent production rates (those actually measured) to differ from those produced in the pure mineral (which we here refer to as in-situ rates).

The distinction between apparent and in-situ production rates arises from redistribution of high energy spallation products within the crystals in a rock. The energy spectrum of spalled  $^3\text{He}$  (and  $^3\text{H}$ , which decays to  $^3\text{He}$  and typically accounts for half to a third of cosmogenic  $^3\text{He}$  production [6]) is not well known, but is likely to be broad and have a maximum of many MeV [23]. Such energies are high enough that nuclei produced in one crystal may come to rest in another. For example, a spalled  $^3\text{He}$  nucleus with 10 MeV of kinetic energy has a range of

nearly 50  $\mu\text{m}$  in common minerals, while a  $^3\text{H}$  nucleus of the same energy has a range of almost 200  $\mu\text{m}$  [24]. In the case of the accessory minerals investigated here, these ranges are similar to crystal dimensions. If the cosmogenic production rate inside the crystal and in its host are identical, then import and export of  $^3\text{He}$  (and  $^3\text{H}$ ) will be in balance and the effect can be ignored. However for trace minerals with lower in-situ  $^3\text{He}$  production rates than the common constituents of the host rock (see Table 3), the apparent production rate will lie between the in-situ production rate of that mineral and that of its host phases.

The relevant variables that dictate the apparent production rate are the in-situ production rates, and the ratio of the stopping range of the spallation nucleus to the dimensions of the crystal. If this ratio is large, there will be substantial implantation or ejection. This problem is analogous to  $\alpha$ -ejection in (U–Th)/He dating, and can be approached using the same mathematical formulations.

Fig. 4 shows this effect as a function of the ratio of the stopping range ( $S$ ) to the crystal radius ( $R$ ) and was computed by combining the  $\alpha$ -ejection expression for a sphere [25] with the analogous formula for  $\alpha$  implantation into a sphere [26]:

$$P_a = P_i[1 - 0.75(S/R) + 0.625(S/R)^3] + P_h[0.75(S/R) - 0.625(S/R)^3] \quad (1)$$

Here  $P_a$  is the apparent production rate and  $P_i$  and  $P_h$  are the in-situ production rates in the mineral of interest and its host. To make the example concrete the calculation

assumes the theoretical production rates shown in Table 3, in particular assuming a host of granitic (or rhyolitic) composition. These assumptions are only meant to be illustrative. The important features of Fig. 4 are 1) if  $(S/R)$  exceeds 2, then all the  $^3\text{He}$  must be implanted and the apparent production rate is that of the host; 2) As  $S/R$  approaches zero, the apparent production rate approaches that of purely in-situ production. When  $S$  and  $R$  are comparable, the exact grain size analyzed controls the apparent production rate. For example, in the case of zircon, a factor of 2 decrease in grain size from  $S/R=0.5$  to  $S/R=1.0$  would lead to a 20% increase in the apparent production rate. The comparable effect is only 8% for apatite because the in-situ production rate in apatite and host are fairly similar. Accurate calculation of the effect is more complex than illustrated here because there will be a range of spallation energies from different target elements and thus a range in  $S$  values (further compounded by the different stopping ranges expected for  $^3\text{He}$  and  $^3\text{H}$ ).

The fact that the measured apparent production rates differ among apatite, titanite and zircon (Table 3) demands that  $S/R$  does not exceed 2, i.e., not all  $^3\text{He}$  is implanted. Given that the grain size of these minerals is of order  $R \sim 75 \mu\text{m}$ , this observation implies an effective value for  $S$  of less than  $\sim 150 \mu\text{m}$ , probably significantly less.

The single experiment on size-sorted zircons of fraction D1\_D2 (Table 1) indicates a decrease in  $^3\text{He}$  concentration from 64.4 to 63.7 to 55.7 Matoms/g as mass-weighted mean grain size increases from 53 to 91 to 111  $\mu\text{m}$ , respectively. The  $^3\text{He}$  concentrations differ only slightly beyond  $2\sigma$  uncertainty, but imply an

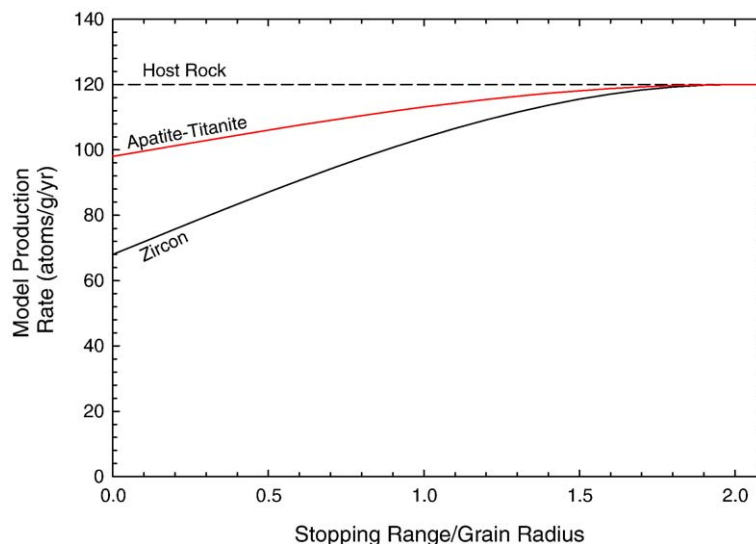


Fig. 4. Relationship between stopping range of spallation  $^3\text{He}$  or  $^3\text{H}$  ( $S$ ) and the radius of the grains ( $R$ ) being analyzed. Dashed line indicates production rate assumed for granitic host rock. In-situ production rates for apatite, titanite, and zircon are as shown in Table 3. Implantation from the host causes apparent  $^3\text{He}$  production rates to lie on the indicated curves.

increase of about 14% for a doubling in  $(1/R)$ . This is in good agreement with the zircon trajectory in Fig. 4 for values of  $S/R$  less than 2.

A detailed analysis of unbroken size-sorted grains is required to further quantify the role of grain size on apparent production rate, and in particular to evaluate the effective stopping range  $S$  for spallation  $^3\text{He}$ . Regardless, the two messages of Fig. 4 are that grain size is likely to influence the apparent production rate, and the magnitude of the effect is about  $\pm 10\%$  across a very large range in grain size (slightly more for zircon, substantially less for apatite and titanite). From a practical perspective high precision surface exposure dating of these phases may require analysis of size-sorted grains both for calibration and chronometry. Nevertheless the apparent production rates in Table 2 are likely to be broadly applicable because they were obtained on size fractions typical of the grain sizes found in common rock types.

In the case of the Bolivian core the evidence suggests that all  $^3\text{He}$  is cosmogenic, but this may not be a general result. The  $^3\text{He}$  concentration of a mineral reflects the sum of cosmogenic and non-cosmogenic (nuclear, fluid inclusion) components:

$$^3\text{He} = \int_0^{T_e} P_c dt + \int_0^{T_r} (F_n P_n + F_i P_{n,h} + F_{\text{SF}} P_{\text{SF}}) dt + ^3\text{He}_o \quad (2)$$

where

$P_c$	apparent cosmogenic $^3\text{He}$ production rate
$T_e$	apparent surface exposure age
$P_n$	in-situ nucleogenic $^3\text{He}$ production rate (from $^6\text{Li}$ )
$F_n$	fraction of in-situ nucleogenic $^3\text{He}$ production retained by crystal
$P_{n,h}$	nucleogenic $^3\text{He}$ production rate in host rock (from $^6\text{Li}$ )
$F_i$	fraction of host nucleogenic $^3\text{He}$ production injected into crystal
$P_{\text{SF}}$	spontaneous fission $^3\text{He}$ production rate
$F_{\text{SF}}$	fraction of spontaneous fission $^3\text{He}$ retained by crystal
$T_r$	accumulation period for nucleogenic/fissionogenic helium = $(\text{U} - \text{Th})/\text{He}$ age
$^3\text{He}_o$	initial (non-nucleogenic) $^3\text{He}$ , e.g., in fluid inclusions

To obtain reliable exposure ages the first term of this equation must either greatly exceed the sum of the second two terms, or the sum must be determined independently (e.g., on an unexposed sample). Here we consider the probable magnitude of the non-cosmogenic components.

Studies of cosmogenic  $^3\text{He}$  in olivines from basalts highlight the fact that mantle  $^3\text{He}$  can be carried in fluid inclusions. This excess- $^3\text{He}$  can be removed prior to analysis by crushing the olivines sufficiently small (typically  $< 100 \mu\text{m}$ ) that the inclusion gas is released [27]. Inclusion  $^3\text{He}$  is unlikely to be a problem for cosmogenic dating of apatite, titanite and zircon. The most common lithologies we wish to exposure date spend extensive periods in magma chambers. Such bodies outgas and cool sufficiently slowly that inclusion-borne gas is lost from crystals both by diffusion and by inclusion annealing. In addition, crystals of accessory minerals are already so fine that inclusions likely carry only a small amount of  $^3\text{He}$ , i.e., the crystals are already smaller than the size to which olivines are crushed to release inclusion gas. This component may nevertheless be important when the cosmogenic  $^3\text{He}$  concentration is low.

A concern unique to determination of cosmogenic  $^3\text{He}$  in U-rich phases is the production of  $^3\text{He}$  from fission. Spontaneous binary fission of  $^{238}\text{U}$  does not produce  $^3\text{He}$ . However, ternary fission occurs in about 1 in 500 fission decays, and about 5% of ternary decays emit a  $^3\text{H}$  nucleus [28]. Using these figures and a spontaneous fission half life of  $8 \times 10^{15}$  years, the instantaneous production rate of  $^3\text{He}$  from fission,  $P_{\text{SF}} = 2 \times 10^{-5}$  atoms  $^3\text{He}/\text{g/ppmU}/\text{yr}$ . The  $^3\text{H}$  nuclei are emitted from the fissioning nucleus with a mean kinetic energy of  $8.5 \pm 2.4$  MeV ( $1\sigma$ , [28]), and as a consequence significant ejection from small crystals will occur.  $^3\text{H}$  nuclei of this energy will have a mean range of  $\sim 160 \mu\text{m}$  in apatite, titanite and zircon according to the SRIM software [24]. This is large enough that ejection will be large ( $F_{\text{SF}}$  is likely to be very close to zero), so spontaneous fission is not a serious problem.

Nucleogenic  $^3\text{He}$  produced by the reaction  $^6\text{Li}(n,\alpha)^3\text{H}$  is the largest probable source of non-cosmogenic  $^3\text{He}$ . The production rate of  $^3\text{He}$  ( $P_n$ ) from this reaction is a function of the Li concentration within the crystal and the neutron flux in the rock. The neutron flux is controlled by 1) U and Th decays, which produce neutrons via spontaneous fission and more importantly from  $(\alpha,n)$  reactions on light elements, and 2) the concentration of neutron absorbers within the rock [29–31]). Although the production of neutrons will be highly localized within the radioactive minerals, because the neutron range is long and the radioactive phases are usually very small and widely distributed, the neutron flux will be essentially homogeneous at a hand-sample scale. Thus the production rate of  $^3\text{He}$  from  $^6\text{Li}$  will be completely independent of the U, Th concentration of any specific mineral, i.e., it is no higher in a U-rich zircon than in a nearby quartz crystal with the same Li concentration.

The  ${}^6\text{Li}$  reaction ejects the  ${}^3\text{H}$  nucleus with 2.7 MeV of energy. These particles have a stopping range of about 30  $\mu\text{m}$  in common minerals [24]. Using the calculations for alpha ejection correction in (U–Th)/He dating [25], this range will cause ejection losses for grains of  $>50 \mu\text{m}$  minimum dimension such that  $F_n$  will range from 0.2 to unity.

Ion probe measurements indicate sub-ppm concentrations of Li in apatite [11] and such low values likely apply to titanite and zircon as well. However as with cosmogenic production, we also need to consider implantation of tritium from Li in the host rock,  $P_{n,i}$ . The sum of ejection and implantation of nucleogenic tritium will obey a relationship similar to that for spallation products in Eq. (1). The only difference is that  $S$  is well-known to be  $\sim 30 \mu\text{m}$ . For example, Eq. (1) shows that assuming zero Li in the crystal of interest and 20 ppm in the host (a reasonable granitoid value [32]), the  ${}^3\text{He}$  production in spheres of 30, 75, and 200  $\mu\text{m}$  radius will be equivalent to an “effective” Li content of 14, 6 and 2 ppm, respectively (i.e.,  $F_i$  values of 0.7, 0.3, and 0.1). Thus it seems likely that for the small grains typical of apatite, titanite and zircon, implantation rather than in-situ production will be the dominant factor controlling the nucleogenic  ${}^3\text{He}$  concentration.

Translating the effective Li concentration into a  ${}^3\text{He}$  production rate requires knowledge of the major and trace element composition of the rock. Formulae presented by Andrews [30] and Lal [31] suggest a  ${}^3\text{He}$  production rate of  $P_n \sim 0.014 \text{ at/g/yr}$  per ppm Li for average granite or rhyolite, but this number probably varies at least over a factor of a few even among felsic igneous rocks. This variability mostly reflects variations in trace element composition (especially of U, Th, B, Sm, and Gd). Importantly, these authors assumed a homogenous distribution of elements in their calculations. At the length scale of  $\alpha$  stopping ( $\sim 20 \mu\text{m}$  [25]) across which  $(\alpha, n)$  reactions occur, most rocks are chemically heterogeneous. In particular a large fraction of  $\alpha$  particles will be produced and stopped in minerals with composition different from that of the whole rock. As a consequence the relevant composition for neutron production via  $(\alpha, n)$  reactions is that of the U, Th bearing phases. These phases tend to be enriched in heavier elements that do not participate in  $(\alpha, n)$  reactions [33]. For example, if one assumes that all  $\alpha$  particles are produced (and stopped) in zircon rather than in homogenous granite composition, the neutron production would drop by almost 80% according to [29]. Martel et al. reached a similar conclusion [34]. These factors taken together suggest that the nucleogenic  ${}^3\text{He}$  production rate is probably uncertain at about the order of magnitude level, and is probably significantly lower than the pre-

viously suggested value of  $\sim 0.014 \text{ at/g/yr}$  per ppm Li in granite or rhyolite.

The amount of nucleogenic  ${}^3\text{He}$  depends not only on the effective Li concentration, but on the duration over which helium is retained, which is equivalent to the (U–Th)/He age [10]. Taking the case of 6 ppm of effective Li in a 75  $\mu\text{m}$  grain (see above) and using the high end production rate of  $\sim 0.014 \text{ at/g/yr}$  per ppm Li as an order-of-magnitude illustration, the nucleogenic  ${}^3\text{He}$  production would be 84 katoms/g/Myr, which is equivalent to  $\sim 800$  years of SLHL exposure in apatite per Myr of (U–Th)/He age. For the 7.5 Ma Bolivian ignimbrite this production rate would yield 0.6 Matoms/g, which is  $<15\%$  of the  ${}^3\text{He}$  measured in even the deepest samples.

Given the very large uncertainty and variability in the effective Li content of the trace phases and in the neutron production/absorption rate in the host rock, and large variations in (U–Th)/He ages of phases that might be attempted for surface exposure dating, it will be necessary to analyze unexposed samples to quantitatively assess the significance of nucleogenic  ${}^3\text{He}$ .

## 5. Conclusions

Results from the Bolivia drill core demonstrate that cosmogenic  ${}^3\text{He}$  can be readily measured in few-mg quantities of apatite, titanite, and zircon and provide the first empirical estimates of the  ${}^3\text{He}$  apparent production rate in these phases: respectively 112, 97 and 87 atoms/g/yr with a  $2\sigma$  uncertainty of  $\sim 20\%$ . The attenuation length scale of  ${}^3\text{He}$  of  $180 \pm 11 \text{ g/cm}^2$  is identical to that of Ne in coexisting quartz and similar to that of other cosmogenic isotopes produced by neutron spallation. There is no evidence for a significant muon-produced  ${}^3\text{He}$  component at these shallow depths, nor for other sources of  ${}^3\text{He}$  in any of these phases.

While these data suggest the utility of cosmogenic  ${}^3\text{He}$  dating of these minerals, several key issues remain. First, further work is required to establish the stopping distance of spallation  ${}^3\text{He}$  and  ${}^3\text{H}$  in common minerals. Stopping distances are probably comparable to the size of the crystals being analyzed, and this will cause the apparent production rate to lie between that of in-situ production in the host rock and that in the pure mineral being analyzed. Data presented here suggest the effect is likely smaller than about  $\pm 10\%$  in apparent production rate for common apatite, titanite and zircon grain sizes.

More important is the possible presence of nucleogenic  ${}^3\text{He}$  from the  ${}^6\text{Li}(n, \alpha)$  reaction. While this source of  ${}^3\text{He}$  is negligible in the Bolivian core because it has such a young (U–Th)/He age, many dating targets will be far older. Our calculations suggest several sources of

uncertainty for estimating the magnitude of nucleogenic  $^3\text{He}$  production. As with cosmogenic production, both in-situ production and implantation from Li in surrounding grains must be considered. The balance between these two sources depends on the contrast in Li concentration between them, and on the grain size being analyzed. In addition, variations in the composition and grain size of the U,Th bearing phases and in the major and trace element composition of the host rock can have order of magnitude level effects on the rate of nucleogenic  $^3\text{He}$  production. An empirical approach of analyzing  $^3\text{He}$  concentrations in unexposed samples is required to further assess the magnitude of this effect.

### Acknowledgements

We thank C. Garzione for field assistance and thoughtful discussion and Don Burnett for numerous helpful conversations regarding nuclear processes. We also acknowledge two anonymous reviewers. This research was supported by the National Science Foundation EAR (0350396, Libarkin); EAR (0408526, Farley); and by funds provided to SM by Harvard University.

### Appendix A. Supplementary data

Supplementary data associated with this article can be found, in the online version, at [doi:10.1016/j.epsl.2006.06.008](https://doi.org/10.1016/j.epsl.2006.06.008).

### References

- [1] J.C. Gosse, F.M. Phillips, Terrestrial in situ cosmogenic nuclides: theory and application, *Quat. Sci. Rev.* 20 (2001) 1475–1560.
- [2] D. Lal, Cosmic ray labeling of erosion surfaces: in situ nuclide production rates and erosion models, *Earth Planet. Sci. Lett.* 104 (1991) 424–439.
- [3] P.R. Bierman, Using in-situ produced cosmogenic isotopes to estimate rates of landscape evolution — a review from the geomorphic perspective, *J. Geophys. Res.-Solid Earth* 99 (1994) 13885–13896.
- [4] S. Niedermann, Cosmic-ray-produced noble gases in terrestrial rocks: dating tools for surface processes, noble gases in geochemistry and cosmochemistry, *Rev. Mineral. Geochem.* 47 (2002) 731–784.
- [5] D.L. Shuster, K.A. Farley, Diffusion kinetics of proton-induced  $^{21}\text{Ne}$ ,  $^3\text{He}$  and  $^4\text{He}$  in quartz, *Geochim. Cosmochim. Acta* 69 (2005) 2349–2359.
- [6] F. Kober, S. Ivy-Ochs, I. Leya, H. Baur, T. Magna, R. Wieler, P.W. Kubik, In situ cosmogenic Be-10 and Ne-21 in sanidine and in situ cosmogenic He-3 in Fe–Ti–oxide minerals, *Earth Planet. Sci. Lett.* 236 (2005) 404–418.
- [7] W.A. Deer, R.A. Howie, J. Zussman, *Double Chain Silicates (Rock Forming Minerals)*, Geological Society, Washington, 1997.
- [8] J.M. Licciardi, P.U. Clark, E.J. Brook, K.L. Pierce, M.D. Kurz, D. Elmore, P. Sharma, Cosmogenic He-3 and Be-10 chronologies of the Late Pinedale northern Yellowstone ice cap, Montana, USA, *Geology* 29 (2001) 1095–1098.
- [9] E. Gayer, R. Pik, J. Lave, C. France-Lanord, D. Bourles, B. Marty, Cosmogenic He-3 in Himalayan garnets indicating an altitude dependence of the He-3/Be-10 production ratio, *Earth Planet. Sci. Lett.* 229 (2004) 91–104.
- [10] K.A. Farley, (U–Th)/He dating: techniques, calibrations, and applications, in: R. Wieler, D. Porcelli (Eds.), *Reviews in Mineralogy and Geochemistry: Noble Gas Geochemistry*, 2002, pp. 819–844.
- [11] K.A. Farley, T.E. Cerling, P.G. Fitzgerald, Cosmogenic He-3 in igneous and fossil tooth enamel fluorapatite, *Earth Planet. Sci. Lett.* 185 (2001) 7–14.
- [12] E.A. du Bray, L.S., W.E. Brooks, B.M. Gamble, J.C. Ratte, D.H. Richter, E. Soria-Escalante, Compositional characteristics of Middle and Upper Tertiary volcanic rocks of the Bolivian Altiplano, *U.S. Geol. Surv. Bull.* 2119 (1995) 30.
- [13] P.W. Reiners, K.A. Farley, H.J. Hickes, He diffusion and (U–Th)/He thermochronometry of zircon: initial results from Fish Canyon Tuff and Gold Butte, *Tectonophysics* 349 (2002) 297–308.
- [14] D.B. Patterson, K.A. Farley, Extraterrestrial  $^3\text{He}$  in seafloor sediments: evidence for correlated 100 kyr periodicity in the accretion rate of interplanetary dust, orbital parameters, and Quaternary climate, *Geochim. Cosmochim. Acta* 62 (1998) 3669–3682.
- [15] J.C. Libarkin, J. Quade, C.G. Chase, J. Poths, W. McIntosh, Measurement of ancient cosmogenic Ne-21 in quartz from the 28 Ma Fish Canyon Tuff, Colorado, *Chem. Geol.* 186 (2002) 199–213.
- [16] S. Niedermann, T. Graf, K. Marti, Mass spectrometric identification of cosmic-ray produced neon in terrestrial rocks with multiple neon components, *Earth Planet. Sci. Lett.* 118 (1993) 65–73.
- [17] S. Niedermann, The Ne-21 production rate in quartz revisited, *Earth Planet. Sci. Lett.* 183 (2000) 361–364.
- [18] E.T. Brown, E.J. Brook, G.M. Raisbeck, F. Yiou, M.D. Kurz, Effective attenuation lengths of cosmic-rays producing Be-10 and Al-26 in quartz — implications for exposure age dating, *Geophys. Res. Lett.* 19 (1992) 369–372.
- [19] P. Sarda, T. Staudacher, C.J. Allegre, A. Lecomte, Cosmogenic neon and helium at Reunion: measurement of erosion rate, *Earth Planet. Sci. Lett.* 119 (1993) 405–417.
- [20] J. Masarik, R.C. Reedy, Terrestrial cosmogenic–nuclide production systematics calculated from numerical simulations, *Earth Planet. Sci. Lett.* 136 (1995) 381–395.
- [21] M.D. Kurz, In situ production of terrestrial cosmogenic helium and some applications to geochronology, *Geochim. Cosmochim. Acta* 50 (1986) 2855–2862.
- [22] J. Masarik, R. Reedy, Monte Carlo simulation of in-situ produced cosmogenic isotopes, *Radiocarbon* 38 (1996) 163.
- [23] G. Friedlander, J.W. Kennedy, J.M. Miller, *Nuclear and Radiochemistry*, Wiley-Interscience, New York, 1981 684 pp.
- [24] J.F. Ziegler, *Stopping and Range of Ions in Matter (SRIM)*, 2003.
- [25] K.A. Farley, R.A. Wolf, L.T. Silver, The effects of long alpha-stopping distances on (U–Th)/He ages, *Geochim. Cosmochim. Acta* 60 (1996) 4223–4229.
- [26] T.J. Dunai, J. Wijbrans, Long-term cosmogenic  $^3\text{He}$  production rates (152 ka–1.35 Ma from  $^{40}\text{Ar}/^{39}\text{Ar}$  dated basalt flows at 29°N latitude, *Earth Planet. Sci. Lett.* 176 (2000) 147–156.
- [27] M.D. Kurz, D. Colodner, T.W. Trull, R.B. Moore, K. O'Brien, Cosmic ray exposure dating with in situ produced cosmogenic  $^3\text{He}$ : results from Hawaiian lava flows, *Earth Planet. Sci. Lett.* 97 (1990) 177–189.

- [28] I. Halpern, 3 fragment fission, *Annu. Rev. Nucl. Sci.* 21 (1971) 245.
- [29] J.N. Andrews, R.L.F. Kay, Natural production of tritium in permeable rocks, *Nature* 298 (1982) 361–363.
- [30] J.N. Andrews, The isotopic composition of radiogenic helium and its use to study groundwater movement in confined aquifers, *Chem. Geol.* 49 (1985) 339–351.
- [31] D. Lal, Production of  $^3\text{He}$  in terrestrial rocks, *Chem. Geol.* 60 (1987) 89–98.
- [32] S. Gao, T.C. Luo, B.R. Zhang, H.F. Zhang, Y.W. Han, Z.D. Zhao, Y.K. Hu, Chemical composition of the continental crust as revealed by studies in East China, *Geochim. Cosmochim. Acta* 62 (1998) 1959–1975.
- [33] Y. Feige, B.G. Oltman, J. Kastner, Production rates of neutrons in soils due to natural radioactivity, *J. Geophys. Res.* 73 (1968) 3135–3138.
- [34] D.J. Martel, D.R. O’Nions, D.R. Hilton, E.R. Oxburgh, The role of element distribution in production and release of radiogenic helium: the Carnmenellis Granite, Southwest England, *Chem. Geol.* 88 (1990) 207–221.